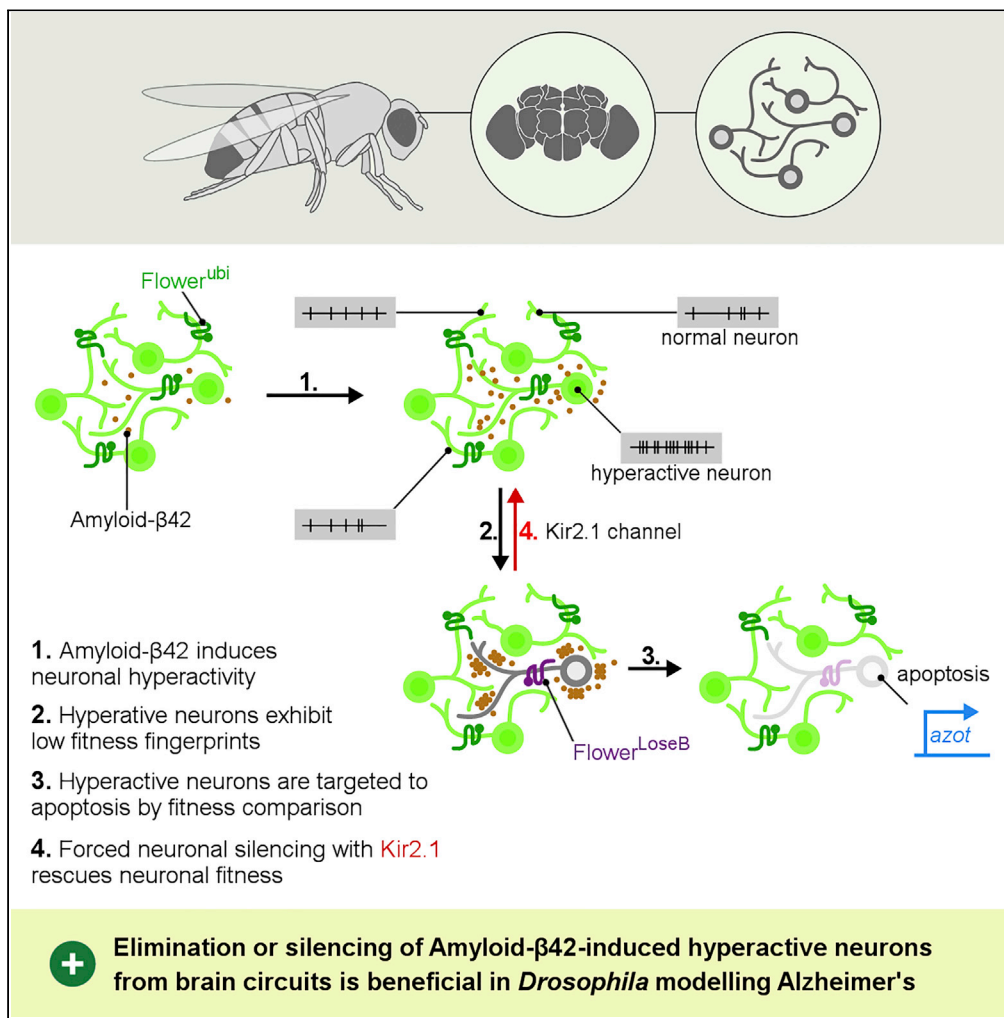


Article

# Neuronal Selection Based on Relative Fitness Comparison Detects and Eliminates Amyloid- $\beta$ -Induced Hyperactive Neurons in *Drosophila*



Dina S. Coelho,  
Eduardo Moreno

eduardo.moreno@research.  
fchampalimaud.org

**HIGHLIGHTS**

Expression of human Amyloid- $\beta$  generates hyperactive neurons in the *Drosophila* brain

Hyperactive neurons up-regulate the low fitness indicators, Flower<sup>LossB</sup> and Azot

Fitness comparison between neurons targets hyperactive neurons to apoptosis

Forced neuronal silencing improves brain fitness in Amyloid- $\beta$ -flies



## Article

Neuronal Selection Based on Relative Fitness Comparison Detects and Eliminates Amyloid- $\beta$ -Induced Hyperactive Neurons in *Drosophila*Dina S. Coelho<sup>1</sup> and Eduardo Moreno<sup>1,2,\*</sup>

## SUMMARY

During adult life, damaged but viable neurons can accumulate in the organism, creating increasingly heterogeneous and dysfunctional neural circuits. One intriguing example is the aberrant increased activity of cerebral networks detected in vulnerable brain regions during preclinical stages of Alzheimer's disease. The pathophysiological contribution of these early functional alterations to the progression of Alzheimer's disease is uncertain. We found that a unique cell selection mechanism based on relative fitness comparison between neurons is able to target and remove aberrantly active neurons generated by heterologous human amyloid- $\beta$  in *Drosophila*. Sustained neuronal activity is sufficient to compromise neuronal fitness and upregulate the expression of the low fitness indicators Flower<sup>LoseB</sup> and Azot in the fly. Conversely, forced silencing of neurons restores brain fitness and reduces amyloid- $\beta$ -induced cell death. The manipulation of this cell selection process, which was already proved to be conserved in humans, might be a promising new avenue to treat Alzheimer's.

## INTRODUCTION

Neurons are particularly vulnerable to external and internal insults as they are post-mitotic, long-lived cells with intense vesicle trafficking. During adult life, suboptimal but viable neurons can accumulate in the organism creating increasingly heterogeneous and dysfunctional neural circuits that may originate disease (Frere and Slutsky, 2018; Coelho et al., 2019). One relevant case study is the aberrant activity of individual neurons and complex cerebral networks detected in patients and mouse models at early stages of Alzheimer's disease (AD) (Busche and Konnerth, 2015; Palop and Mucke, 2010; Stargardt et al., 2015; Zott et al., 2018). fMRI studies revealed abnormally increased activity and deactivation defects in brain circuits vulnerable to AD, mainly the hippocampus and the default mode network, which are important for memory encoding and introspective thought, respectively (Bookheimer et al., 2000; Dickerson et al., 2005; Quiroz et al., 2010; Sperling et al., 2009). These functional alterations were detected at preclinical stages, sometimes even decades before the overt onset of symptoms, in groups at risk for AD, including asymptomatic individuals with high amyloid- $\beta$  burden, pre-symptomatic carriers of familial AD mutations, and subjects with genetic predisposition for late-onset AD (Filippini et al., 2009; Mondadori et al., 2006; Quiroz et al., 2010; Reiman et al., 2012; Sperling et al., 2009). In agreement, two-photon Ca<sup>2+</sup> imaging showed a great abundance of hyperactive neurons in the cortex and the hippocampus of mouse models of AD, strikingly clustering near amyloid plaques (Busche et al., 2008; 2012; Grienberger et al., 2012; Rudinskiy et al., 2012).

In *Drosophila*, a unique mechanism of active cell selection is able to detect and eliminate suboptimal neurons based on their fitness status (Rhiner et al., 2010; Merino et al., 2013; Moreno et al., 2015). This mechanism generally known as "cell competition" has important physiological consequences for the organism such as to sculpt the visual system during development, to replace old or damaged brain tissue during aging or upon injury, and to protect long-term memory (Merino et al., 2013, 2015, 2016; Moreno et al., 2015; Coelho et al., 2018).

Neurons compare relative fitness among themselves through external clues exhibited at their membranes called "fitness fingerprints." The different isoforms encoded by the conserved protein Flower compose these "fingerprints" and mediate the elimination of less-fit cells both in *Drosophila* and in humans (Madan et al., 2019; Petrova et al., 2012; Rhiner et al., 2010). We recently described that overproduction of human

<sup>1</sup>Cell Fitness Lab, Champalimaud Centre for the Unknown, Av. Brasília, 1400-038 Lisboa, Portugal

<sup>2</sup>Lead Contact

\*Correspondence: eduardo.moreno@research.fchampalimaud.org  
<https://doi.org/10.1016/j.isci.2020.101468>



amyloid- $\beta$ , a pathogenic peptide forming extracellular brain plaques in AD (for abbreviation A $\beta$ ), impairs neuronal brain fitness and that A $\beta$ -damaged neurons are removed by fitness-mediated apoptosis in *Drosophila* (Coelho et al., 2018). An important unsolved question in this study, and in AD research in general, is how broad expression of A $\beta$  mounts an insult that predisposes particular neurons to death and damage, whereas other neurons are less vulnerable.

## RESULTS

### Amyloid- $\beta$ Generates Hyperactive Neurons in the *Drosophila* Brain

We hypothesized that A $\beta$ -induced damaged neurons that are eliminated by fitness comparison in *Drosophila* correspond to dysfunctional neurons with lower fitness status (Coelho et al., 2018). To find and characterize these neurons, we sought out to monitor neural activity with the genetically encoded Ca<sup>2+</sup> sensor, GCaMP6s (Chen et al., 2013). We induced the expression of the human 42-aminoacid amyloid- $\beta$  peptide (A $\beta$ 42) under the control of the *Mef2-Gal4.247* driver using the UAS-GAL4 system (hereafter referred to as *MB247>A $\beta$ 42*). This driver is specific for mature neurons of the mushroom body (MB), a critical center for learning and memory in flies (Aso et al., 2014). On average, we detected a higher baseline intensity of GCaMP6s fluorescence per neuron and per mushroom body calyx in two-photon images of *ex vivo* brains from A $\beta$ 42-flies compared with control flies (Figures 1A–1C, *MB247>+* = 891.4 [n = 141] versus *MB247>A $\beta$ 42* = 1464 [n = 160]; and Figure S1A, *MB247>+* = 1 [n = 15] versus *MB247> A $\beta$ 42* = 1.38 [n = 16]). When recording videos of Ca<sup>2+</sup> imaging in non-stimulated *ex vivo* brains, we registered that A $\beta$ 42-brains show neurons with augmented spontaneous activity (Figures S1B and S1C, n.<sup>er</sup> neurons with spontaneous activity: *MB247>+* = 1/10 neurons versus *MB247>A $\beta$ 42* = 10/30 neurons; Videos S1 and S2).

To further characterize dysfunctional neurons in the fly, we employed the CaLexA bipartite system (for calcium-dependent nuclear import of LexA) (Masuyama et al., 2012), which detects increased concentrations of intracellular Ca<sup>2+</sup> evoked by sustained neural activity (Figure 1D). We promptly recognized a very intense signal of CaLexA in discrete soma of Kenyon cells in *MB247>A $\beta$ 42* adult flies at 10 days after eclosion (Figures 1E–1G, mean number of saturated pixels: *MB247>+* = 16.75 [n = 16] versus *MB247>A $\beta$ 42* = 314.8 [n = 12]). We did not observe a specific pattern in the distribution of CaLexA-activating neurons, as different Kenyon cells were randomly labeled in each brain. Taking into account our previous recordings with GCaMP6s showing increased spontaneous neuronal activity in the mushroom body of A $\beta$ 42-flies, we think that neurons strongly activating CaLexA correspond to hyperactive neurons. In addition, we confirmed that A $\beta$ 42 does not cause expression of the CaLexA sensor in immature (and thus still not active) neurons of the eye disc (Figures S2A and S2B) or pupal retinas (Figures S2C and S2D). This observation supports the idea that CaLexA expression is only induced by increased activity of neurons and not by deregulated Ca<sup>2+</sup> fluxes between intracellular compartments, which might be a secondary consequence of A $\beta$ 42-caused toxicity.

We also found axons exhibiting high levels of CaLexA in the optic lobe of 15-day-old flies when A $\beta$ 42 production was driven by *GMR-Gal4*, suggesting that A $\beta$ 42 can induce hyperactive neurons in different brain regions (Figures 1H–1J). Activation of CaLexA in *GMR > A $\beta$ 42*-flies was accompanied by a 52% increase in the concentration of the excitatory neurotransmitter glutamate in the optic lobe, raising the hypothesis that aberrant neuronal activity promoted by A $\beta$ 42 is correlated with an excessive brain excitability (Figures S2E–S2G, mean fluorescence intensity of glutamate: *GMR > lacZ* = 117.8 [n = 24] versus *GMR > A $\beta$ 42* = 179.1 [n = 22]).

We then investigated the fitness status of A $\beta$ 42-induced hyperactive neurons by checking the expression of the “poor fitness” membrane fingerprint, Flower<sup>LOSEB</sup>, and the expression of azot, a gene that indispensably targets less-fit cells to death (Merino et al., 2015). Approximately 12.4% of Kenyon cells activating CaLexA displayed cytoplasmic positive signal for the translational reporter Flower<sup>LOSEB</sup>:Myc (derived from a tagged genomic rescue construct, Yao et al., 2009) (Figure 1K). We also found co-localization between CaLexA and the fluorescent reporter Flower<sup>LOSEB</sup>:mCherry (produced from a *knockin* of mCherry into the endogenous *flower* locus) in the membranes of cell bodies and projections of Kenyon cells (Figure S2H). Moreover, an Azot:mCherry fusion protein was expressed in CaLexA-positive neurons, particularly when CaLexA was highly activated (Figure 1L) or when apoptosis was genetically suppressed by overexpression of UAS-p35 (Figure S2I). These data suggest that A $\beta$ 42-induced hyperactive neurons exhibit low fitness markers and might be subjected to negative cell selection via fitness comparison.

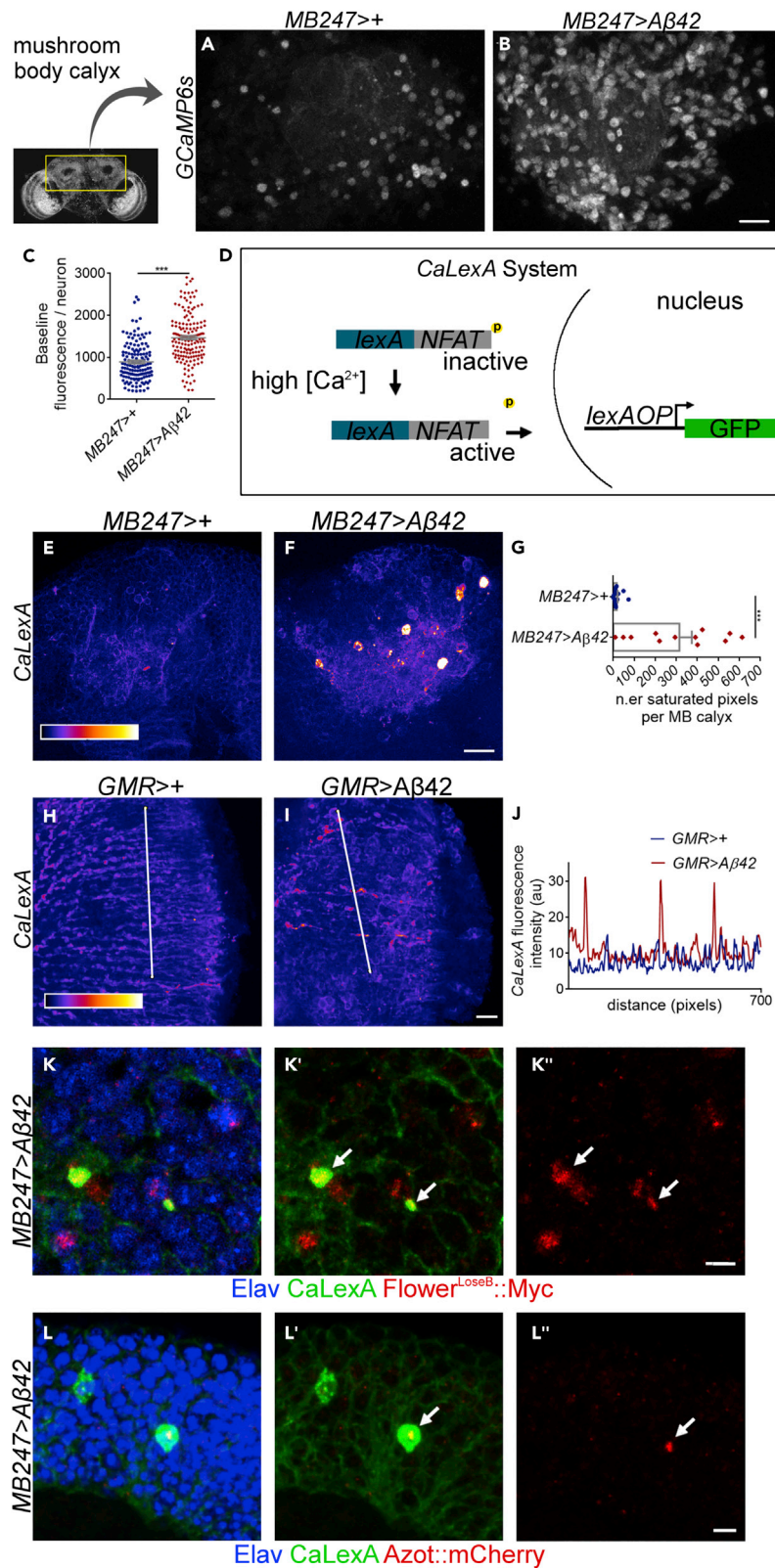


### Figure 1. Amyloid- $\beta$ Generates Hyperactive Neurons in the *Drosophila* Brain

(A and B) Two-photon images of GCaMP6s expressed in the mushroom body calyx of ex vivo brains of *MB247>+* flies (A) or *MB247>A $\beta$ 42* flies (B) at 1 week post eclosion. Scale bar, 15  $\mu$ m.

(C) Mean intensity fluorescence of GCaMP6s (arbitrary units) measured at baseline in individual neurons of the mushroom body calyx in non-stimulated ex vivo brains of *MB247>+* flies or *MB247>A $\beta$ 42* flies at 1 week post eclosion. \*\*\*\*p value <0.001, Mann-Whitney U non-parametric test.

(D) Schematic depicting CaLexA, a bipartite system comprising the chimerical transcription factor *lexA::VP16::NFAT* and the responsive element *lexA operator (lexAOP)*. Intracellular accumulation of  $Ca^{2+}$  leads to dephosphorylation of the transcription factor NFAT (Nuclear factor of activated T cells) and its shuttling into the nucleus. Once in the nucleus, *lexA::VP16::NFAT* drives the transcription of GFP downstream of *lexAOP*.

(E and F) CaLexA activation pattern pseudocolored fire in the mushroom body calyx of *MB247>+* (E) or *MB247>A $\beta$ 42* flies (F) at 10 days post eclosion. Scale bar, 10  $\mu$ m.

(G) Quantification of the number of saturated pixels for CaLexA fluorescence counted per mushroom body calyx at 10 days post eclosion for the genotypes: *MB247>+* or *MB247>A $\beta$ 42*. Pixels displaying a fluorescence intensity value above 75% of the maximum intensity value were assumed to be saturated. \*\*\*\*p value <0.001, Mann-Whitney U non-parametric test.

(H and I) CaLexA activation pattern (pseudocolored fire) in the optic lobe of *GMR>+* (H) or *GMR > A $\beta$ 42* (I) flies at 2 weeks old. Scale bar, 5  $\mu$ m.

(J) Intensity profile of CaLexA fluorescence along the lines represented correspondingly in (H) (*GMR>+* flies) and (I) (*GMR > A $\beta$ 42* flies).

(K) CaLexA-activating Kenyon cells (green) are labeled by the low-fitness marker *Flower<sup>LoSeB</sup>:Myc* (red) in *MB247>A $\beta$ 42* brains (arrows). The mean percentage ( $\pm$  SEM) of co-localization is  $12.4 \pm 2.12\%$  per mushroom ( $n = 14$ ). Nuclei labeled by *Elav* are in blue. Scale bar, 5  $\mu$ m.

(L) Kenyon cells showing strong activation of CaLexA (green) are labeled by the low-fitness marker *Azot:mCherry* in *MB247>A $\beta$ 42* brains (arrow). Nuclei labeled by *Elav* are in blue. Scale bar, 5  $\mu$ m.

Data are represented as mean  $\pm$  SEM. See also [Figures S1](#) and [S2](#), [Videos S1](#) and [S2](#).

### Amyloid- $\beta$ -Induced Hyperactive Neurons Undergo Apoptosis Mediated by Relative Fitness Comparison Using Fitness Fingerprints

To follow the temporal distribution of hyperactive neurons overtime (as done before in [Busche et al., 2012](#) and [Hahm et al., 2018](#)), we checked CaLexA expression at three time points: 5, 10, and 15 days post eclosion. We found that the number of hyperactive neurons in the mushroom body increased with age reaching a peak at 10 days old (mean number:  $8.35 \pm 0.58$  neurons per calyx) and decreased in older flies (mean number:  $6.08 \pm 0.54$  neurons per calyx) ([Figure 2A](#)). This observation suggests that hyperactive neurons might be undergoing apoptosis overtime. We registered that 8.3% of CaLexA-positive Kenyon cells were marked by the anti-cleaved *Drosophila* Caspase Protein 1 (DCP1) antibody ([Figure 2B](#)). Furthermore, blockage of cell death by overexpression of *diap1* resulted in a 47.9% increase in the number of hyperactive neurons in *MB247>A $\beta$ 42* flies at 10 days old ([Figures 2C–E](#), *MB247>A $\beta$ 42/+* = 100% [ $n = 21$ ] versus *MB247>A $\beta$ 42/UAS-*diap1** = 147.9% [ $n = 23$ ]). We confirmed that overexpression of *UAS-*diap1** effectively suppressed apoptosis in this model ([Figure 2F](#), *MB247>A $\beta$ 42/+* = 100% [ $n = 25$ ] versus *MB247>A $\beta$ 42/UAS-*diap1** = 57.9% [ $n = 24$ ]). These findings exclude the possibility that increased  $Ca^{2+}$  levels reported by CaLexA are a consequence of cytoplasmic  $Ca^{2+}$  overload following execution of the apoptotic pathway and degradation of  $Ca^{2+}$  channels.

To test the hypothesis that hyperactive neurons are being eliminated from the tissue by fitness-based neuronal selection, we genetically manipulated fitness machinery and used the number of hyperactive neurons marked by CaLexA as a derivative. Downregulation of *flower* expression is known to prevent fitness comparison and to abrogate neuronal selection in other contexts ([Merino et al., 2013](#); [Moreno et al., 2015](#)). To knockdown *flower*, we used two independent RNAi lines: a *Long-Hairpin* that specifically silences *flower<sup>LoSeA/B</sup>* isoforms and a RNAi from the Vienna *Drosophila* Resource Center (VDRC) GD library that targets all *flower* transcripts. Overexpression of the *Long-Hairpin* caused a drastic 75.5% increase in the number of hyperactive neurons detected by CaLexA in *MB247>A $\beta$ 42* heterozygous flies at 10 days ([Figures 2G, 2H, and 2J](#) *MB247>A $\beta$ 42/UAS-*lacZ** = 100% [ $n = 28$ ] versus *MB247>A $\beta$ 42/UAS-*flower<sup>LoSeA/B</sup>** *Long Hairpin* = 175.5% [ $n = 34$ ]). Overexpression of the *flower* dsRNA from VDRC raised by 36.9% the number of CaLexA-positive neurons detected at the same time point ([Figures 2G, 2I, and 2J](#) *MB247>A $\beta$ 42/UAS-*lacZ** = 100% [ $n = 46$ ] versus *MB247>A $\beta$ 42/UAS-*fwe** dsRNA GD = 136.9% [ $n = 32$ ]). Altogether, these results indicate that preventing neuronal fitness comparison in the mushroom body partially rescues *A $\beta$ 42*-induced hyperactive neurons from undergoing apoptosis.

The *Flower<sup>LoSeA</sup>* isoform, but not the *Flower<sup>LoSeB</sup>* isoform, was originally proposed to work as a  $Ca^{2+}$  channel essential for endocytosis of synaptic vesicles at the neuromuscular junction ([Yao et al., 2009](#)). However,

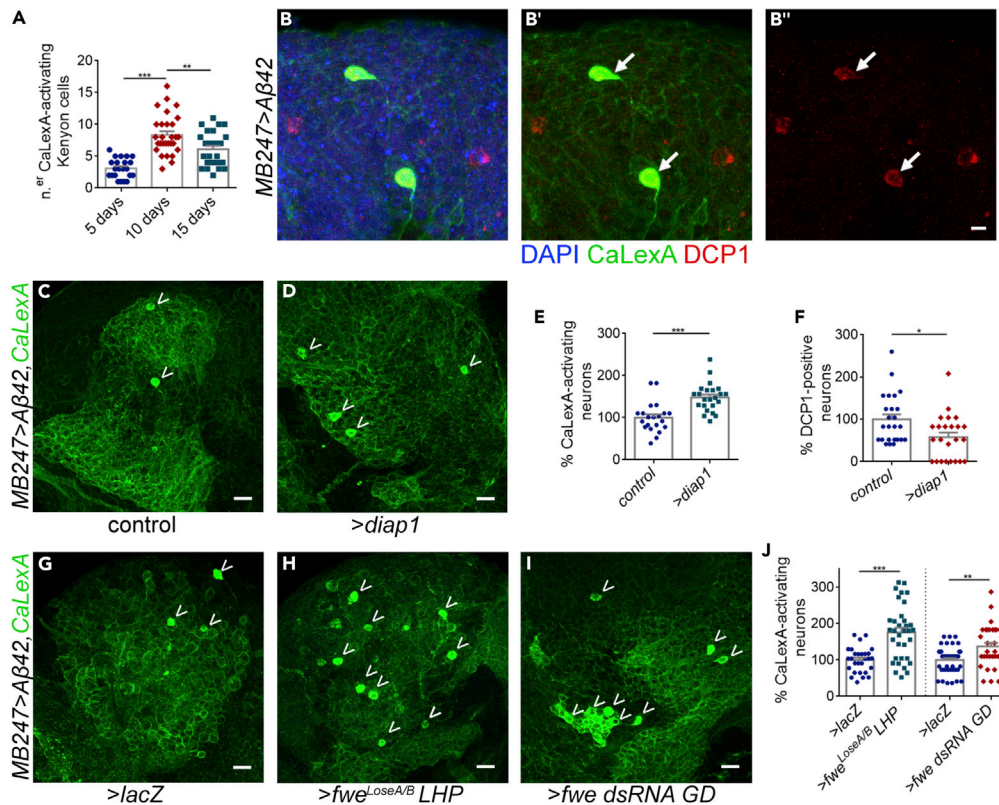


**Figure 2. Amyloid- $\beta$ -Induced Hyperactive Neurons Undergo Apoptosis Mediated by Relative Fitness Comparison Using "Fitness Fingerprints"**

(A) Plot showing the number of hyperactive Kenyon cells as labeled by CaLexA at ages 5, 10, and 15 days post eclosion. Mean number of hyperactive cells  $\pm$  SEM were as follows:  $3.09 \pm 0.33$  ( $n = 22$ ) at 5 days old,  $8.35 \pm 0.58$  ( $n = 29$ ) at 10 days old, and  $6.08 \pm 0.54$  ( $n = 25$ ) at 15 days old. \*\*\*p value  $<0.001$ , \*\*p value  $<0.01$ , one-way ANOVA followed by Holm-Sidak's multiple comparisons test. Note that transgenic flies quantified in (A) carried 3 GFP reporter proteins, LexAop-CD2-GFP ( $1 \times$  GFP) and LexAop-CD8-GFP-2A-CD8-GFP ( $2 \times$  GFP), whereas flies used in (C)–(J) carried only one reporter GFP and thus the number of detectable CaLexA-positive cells is lower in the last cases.

(B) Hyperactive neurons identified by CaLexA (green) show immunolabelling of cleaved DCP1 (in red), a marker of apoptosis execution. The mean percentage ( $\pm$  SEM) of co-localization is  $8.3 \pm 1.94\%$  ( $n = 39$ ) per mushroom body. Scale bar,  $5 \mu\text{m}$ .

(C and D) Neurons activating CaLexA (green soma, arrow heads) accumulate in the mushroom calyx of MB247> A $\beta$ 42 flies when general apoptosis is blocked by overexpression of *UAS-diap1* (D) compared with 10-day-old matched controls (C). Scale bar,  $10 \mu\text{m}$ .

(E) Quantification of neurons labeled by CaLexA in the mushroom body of MB247> A $\beta$ 42/+ flies or MB247> A $\beta$ 42/UAS-*diap1* flies at 10 days of age. \*\*\*p value  $<0.001$ , unpaired Student's t test with Welch's correction.

(F) Quantification of neurons stained by anti-DCP1 antibody in the mushroom body of MB247> A $\beta$ 42/+ flies or MB247> A $\beta$ 42/UAS-*diap1* flies at 10 days of age. \*p value  $<0.05$ , Mann-Whitney U non-parametric test.

(G–I) The number of neurons labeled by CaLexA (bright green soma, arrow heads) is increased in the calyx of MB247> A $\beta$ 42 brains when fitness mediated-apoptosis is suppressed by silencing of *flower* with a *Long-Hairpin RNAi* (H) or with a RNAi transgene from GD library (I), compared with the control genotype expressing  $\beta$ -galactosidase (*UAS-lacZ*, G) at 10 days post eclosion. Scale bar,  $10 \mu\text{m}$ .

(J) Plot representing the percentage of neurons labeled by CaLexA at 10 days post eclosion in the mushroom body of the following genotypes: MB247> A $\beta$ 42/UAS-*lacZ*; MB247> A $\beta$ 42/UAS-*flower*<sup>LoseA/B</sup> *Long Hairpin*, or MB247> A $\beta$ 42/UAS-*fwe dsRNA GD* line. CaLexA numbers were normalized to the number in MB247> A $\beta$ 42/UAS-*lacZ* genotype in each experimental replicate. \*\*\*p value  $<0.001$ ; \*\*p value  $<0.01$ , unpaired Student's t test with Welch's correction. Data are represented as mean  $\pm$  SEM.

See also Figure S3.

further evidence supporting the role of Flower as a  $\text{Ca}^{2+}$  channel is lacking (Chang et al., 2018; Xue et al., 2012; Madan et al., 2019). Nevertheless, to test if increased  $\text{Ca}^{2+}$  levels reported by CaLexA in A $\beta$ 42-expressing flies were associated with  $\text{Ca}^{2+}$  influx through Flower, we performed two types of experiments using the point mutation Flower<sup>LossA[E79Q]</sup>. In this mutant, a glutamic acid substitution in the predicted  $\text{Ca}^{2+}$  selective motif blocks putative  $\text{Ca}^{2+}$  currents (Yao et al., 2009).

In the first experiment, we induced heat-shocked clones marked by GFP in the wing disc, using an act > y+>Gal4 flip-out cassette. Clones overexpressing the mutant form Flower<sup>LossA[E79Q]</sup> were progressively eliminated from the tissue overtime (Figures S3A–S3C, UAS-lacZ clone number = 11.53 [n = 15], UAS-flower<sup>LossA[E79Q]</sup> clone number = 6.4 [n = 14]). In addition, we detected the expression of Azot:mCherry at clone borders overexpressing Flower<sup>LossA[E79Q]</sup>, and DCP1 was more likely expressed at these clone borders than at control borders (Figures S3D and S3E % DCP1 at clone border: UAS-lacZ = 33.46% [n = 15] versus UAS-flower<sup>LossA[E79Q]</sup> = 45.78% [n = 14]). These observations indicate that overexpression of Flower<sup>LossA[E79Q]</sup> is sufficient to target clones for elimination by fitness comparison, independently of a potential  $\text{Ca}^{2+}$  influx. In addition, overexpression of Flower<sup>LossA</sup> under the control of the MB247 driver did not induce changes in  $\text{Ca}^{2+}$  levels as detected by CaLexA (Figures S3F and S3G), making a solid argument against the idea that Flower working as a putative  $\text{Ca}^{2+}$  channel mediates increased  $\text{Ca}^{2+}$  fluxes detected by CaLexA.

### Sustained Activation of Neurons with a Thermosensitive Channel Induces Up-Regulation of the Low Fitness Indicator, Flower<sup>LossB</sup>, and Triggers Apoptosis

Patients with AD are more vulnerable to epileptic seizures, which result from an excessive synchronization of neuronal networks and increased neuronal excitability (Palop, 2009; Palop and Mucke, 2010; Vossel et al., 2013, 2016). To mimic in *Drosophila* the excessive excitability and hyperactivity observed in patients with AD, we ectopically expressed the excitatory cation channel (TRPA1) (transient receptor potential A1) (Figure 3A). TRPA1 is a thermosensitive channel that promotes depolarization of neurons and action potential firing at elevated temperatures (>25°C) but maintains a closed conformation at lower temperatures (Figure 3A) (Hamada et al., 2008). TRPA1 was driven either under the control of a cholinergic promoter (*chat-Gal4*) for mosaic expression in the brain or by *GMR-Gal4* for expression in the optic lobes (Figure 3B). Sustained activation of neurons with TRPA1 for 4 days at 30°C was sufficient to upregulate Flower<sup>LossB</sup> (Figures 3C–3F, *chat* > UAS-TRPA1 22°C = 86.4% [n = 30], *chat* > UAS-lacZ 30°C = 100% [n = 51], *chat* > UAS-TRPA1 30°C = 191.8% [n = 40]; Figures 3G–3J *GMR* > UAS-TRPA1 22°C = 37.78% [n = 30], *GMR* > UAS-lacZ 30°C = 100% [n = 48], *GMR* > UAS-TRPA1 30°C = 139.8% [n = 50]). Increased brain apoptosis was also detected as a consequence of chronic activation of neurons with TRPA1 (Figures 3K–3M, *chat* > UAS-lacZ = 100% [n = 13], *chat* > UAS-TRPA1 = 165.7% [n = 11]; Figures 3N–3P *GMR* > UAS-lacZ = 100% [n = 14], *GMR* > UAS-TRPA1 = 237.5% [n = 13]). This result suggests that neuronal hyperactivity is sufficient to decrease neuronal fitness levels in the fly brain, predisposing less-fit neurons to death.

### Forced Silencing of Neurons Is Sufficient to Improve Cell Fitness Markers and Reduce Amyloid- $\beta$ -Induced Cell Death

Based on the previous results, we reasoned that neuronal silencing might have a physiological benefit in the context of A $\beta$ -induced hyperactivity. To test this hypothesis, we expressed a *kir2.1* transgene in *wild-type* and A $\beta$ 42-transgenic flies and measured neuronal fitness levels. Kir is an Inward-Rectifier K<sup>+</sup> channel that hyperpolarizes neurons and decreases the firing probability of action potentials (Baines et al., 2001). First of all, we confirmed that expression of *kir2.1* per se neither disturbed neuronal differentiation during development (Figures S4A and S4B) nor caused increased apoptosis in the adult brain (Figures S4C–S4E, *GMR* > UAS-lacZ = 100% [n = 8] versus *GMR* > 10XUAS-*kir2.1* = 101% [n = 11]). In particular, the distribution of the neuronal markers Elav (stains nuclei) and Futsch (stains the cytoskeleton) was not affected by *kir2.1* in the neuroepithelium of the eye disc in third instar larvae (Figures S4A and S4B).

Forced neuronal silencing with *kir2.1* downregulated the expression of the Flower<sup>LossB</sup>:mCherry and Azot:mCherry reporters in the brain of *GMR* > A $\beta$ 42 flies compared with controls of the same age (Figures 4A–4E, %Flower<sup>LossB</sup>:mCherry expression: *GMR* > A $\beta$ 42/UAS-lacZ = 183.7% [n = 27] versus *GMR* > A $\beta$ 42/10XUAS-*kir2.1* = 95.48% [n = 27]; Figures 4F–4J, % Azot:mCherry expression: *GMR* > A $\beta$ 42/UAS-lacZ = 153.8% [n = 32] versus *GMR* > A $\beta$ 42/UAS-*kir2.1* = 75.4% [n = 27]). Moreover, silencing of neurons had no impact on Flower<sup>LossB</sup>:mCherry or Azot:mCherry expression measured during normal adulthood, confirming that the rescue of neuronal fitness promoted by *kir2.1* is specific to A $\beta$ 42-induced hyperactivity (Figures 4A, 4B and 4E, Flower<sup>LossB</sup>:mCherry expression: *GMR* > UAS-lacZ = 100% [n = 29] versus *GMR* > 10XUAS-

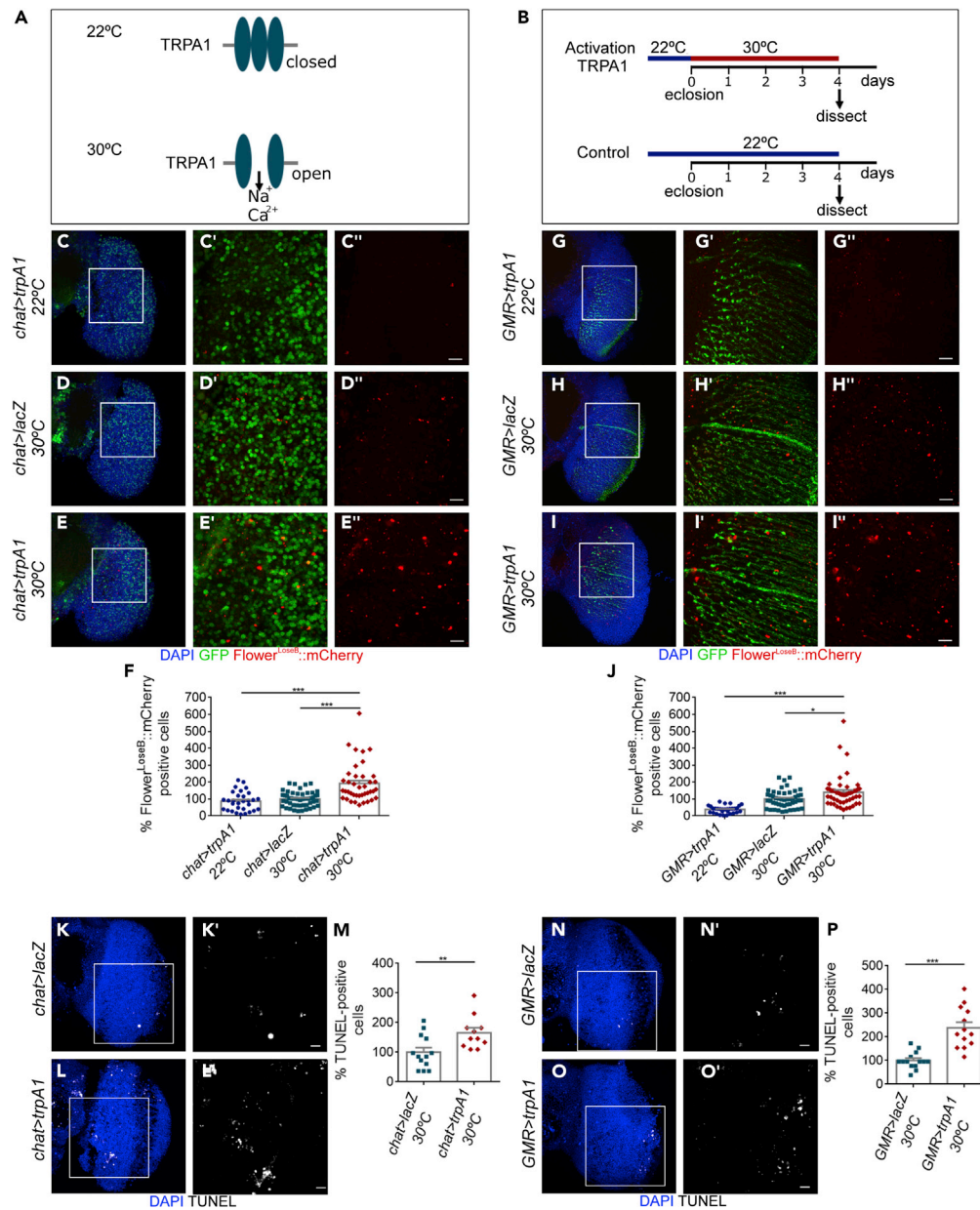


**Figure 3. Sustained Activation of Neurons with a Thermosensitive Channel Induces Up-Regulation of the Low-Fitness Indicator, Flower<sup>LoseB</sup>, and Triggers Apoptosis**

(A) TRPA1 is a cation channel activated by heat. In the wild, the channel allows the fly to avoid noxious heat and to select for preferred ranges of temperatures. At low temperatures (22°C) TRPA1 is closed but shifts to an open conformation at higher temperatures (30°C), leading to the influx of Na<sup>+</sup> and Ca<sup>2+</sup> and induction of action potential firing.

(B) Experimental design followed to induce sustained activation of neurons. After eclosion, flies ectopically expressing TRPA1 were either placed at 30°C to trigger action potential firing or at 22°C for TRPA1 inactivation for 4 days. An additional transgene, *UAS-lacZ*, was expressed at 30°C to serve as a control for expression of Gal4 at high temperatures.

(C–E) The expression of the Flower<sup>LoseB</sup>:mCherry reporter (red) was significantly up-regulated by activation of neurons with TRPA1 (E), compared with controls expressing inactive TRPA1 at 22°C (C) or β-galactosidase (*lacZ*) at 30°C (D). GFP (green) demonstrates the domain of expression for *chat-Gal4* in the optic lobe. The nuclei are in blue. Scale bars, 5 μm in the insets.

(F) Quantification of the percentage of Flower<sup>LoseB</sup>:mCherry-positive cells in the optic lobes of *chat > UAS-lacZ* and *chat > UAS-trpA1* genotypes (placed at 22°C or 30°C). The mean number of Flower<sup>LoseB</sup>:mCherry-positive cells in flies expressing *UAS-lacZ* was considered as 100%. \*\*\*p value < 0.001, Kruskal-Wallis test with Dunn's post hoc paired comparisons.

**Figure 3. Continued**

(G–I) The Flower<sup>LoSeB</sup>:mCherry (red) reporter was significantly up-regulated by activation of neurons with TRPA1 (I), compared with controls expressing inactive TRPA1 at 22°C (G) or  $\beta$ -galactosidase (*lacZ*) at 30°C (H). GFP (green) demonstrates the domain of expression of *GMR-Gal4* in the optic lobe. The nuclei are in blue. Scale bars, 5  $\mu$ m in the insets.

(J) Quantification of Flower<sup>LoSeB</sup>:mCherry-positive cells in the optic lobes of the following genotypes: *GMR > UAS-lacZ* and *GMR > UAS-trpA1* (kept at 22°C or 30°C). The number of Flower<sup>LoSeB</sup>:mCherry-positive cells in flies expressing *UAS-lacZ* was considered as 100%. \*\*\*p value < 0.001, \*p value < 0.05 Kruskal-Wallis test with Dunn's post hoc paired comparisons.

(K and L) Terminal deoxynucleotidyl transferase-mediated dUTP nick-end (TUNEL) labeling of apoptotic cells (white) in the optic lobe of *chat > UAS-lacZ* (K) or *chat > UAS-trpA1* (L) transgenic flies maintained at 30°C after eclosion. DAPI is in blue. Scale bar, 10  $\mu$ m.

(M) Graph depicts the number of TUNEL-positive cells counted in the optic lobe of *chat > UAS-lacZ* or *chat > UAS-trpA1* flies. The number of TUNEL-positive cells for *chat > UAS-lacZ* was used as reference. \*\*p value < 0.01, unpaired Student's t test with Welch's correction.

(N and O) TUNEL labeling of apoptotic cells (white) in the optic lobe of *GMR > UAS-lacZ* (N) or *GMR > UAS-trpA1* (O) flies maintained at 30°C after eclosion. DAPI is in blue. Scale bar, 10  $\mu$ m.

(P) Graph shows the number of TUNEL-positive cells counted in the optic lobe of *GMR > UAS-lacZ* or *GMR > UAS-trpA1* flies. Number of TUNEL-positive cells for *GMR > lacZ* genotype was assumed as 100%. \*\*\*p value < 0.001, unpaired Student's t test with Welch's correction. Data are represented as mean  $\pm$  SEM.

*kir2.1* = 103.5% [n = 31]; [Figures 4F,4G and 4J](#), Azot:mCherry expression: *GMR > UAS-lacZ* = 100% [n = 12] versus *GMR > UAS-kir2.1* = 98.5% [n = 8]).

Remarkably, cell death was also reduced in *GMR > A $\beta$ 42* flies upon neuronal silencing with *kir2.1*. This was tested by terminal deoxynucleotidyl transferase-mediated dUTP nick-end labeling (TUNEL) of apoptotic cells in the adult brain ([Figures 4K–4M](#), *GMR > A $\beta$ 42/UAS-lacZ* = 100% [n = 25] versus *GMR > A $\beta$ 42/10XUAS-kir2.1* = 60.5% [n = 22]) and by analyzing the degenerative phenotype induced by *A $\beta$ 42* in the eye ([Figures S4F–S4H](#), number of necrotic patches: *GMR > A $\beta$ 42/UAS-lacZ* = 11 [n = 26], *GMR > A $\beta$ 42/10XUAS-kir2.1* = 4.8 [n = 32]).

To prevent any possible developmental defect, we restricted *kir2.1* expression to adulthood by using a thermosensitive repressor (*tubGal80<sup>ts</sup>*), which blocks Gal4 activity at lower temperature, 18°C, but allows its expression at higher temperatures (above 29°C) ([McGuire et al., 2004](#)). Again, using conditional expression of *kir2.1* in the adult brain, the number of apoptotic cells present in *GMR > A $\beta$ 42* brains was significantly reduced ([Figures S4I–S4K](#), *GMR > A $\beta$ 42/UAS-tubGal80<sup>ts</sup>* = 100% [n = 47] versus *GMR > A $\beta$ 42/UAS-tubGal80<sup>ts</sup>,UAS-kir2.1* = 67.23% [n = 44]).

Our previous findings demonstrated that *A $\beta$ 42* reduces the fitness status of neurons and that less-fit neurons displaying poor fitness fingerprints are eliminated by apoptosis in *Drosophila* ([Figure 4N](#)) ([Coelho et al., 2018](#)). Data presented here extend this model and suggest that these unfit neurons that are targeted by fitness comparison correspond to aberrantly active neurons ([Figure 4N](#)). Forced silencing of these neurons rescues brain fitness fingerprints and suppresses *A $\beta$ 42*-induced cell death. Altogether, removal of dysfunctional hyperactive neurons is beneficial in *Drosophila* modelling AD, prolonging lifespan, rescuing motor coordination, and protecting against memory loss.

## DISCUSSION

Building upon previous work, we found that a unique cell selection mechanism based on relative fitness comparison is able to detect and remove “excessively active neurons” generated by *A $\beta$ 42* in *Drosophila*. These findings were surprising since events of non-cell autonomous selection (broadly known as cell competition) were originally described in the fly to remove slow proliferating and/or deficient cells from epithelial tissues ([Igaki et al., 2009](#); [Menéndez et al., 2010](#); [Moreno et al., 2002](#); [Vincent et al., 2011](#); [Rodrigues et al., 2012](#); [Moreno and Basler, 2004](#)). In epithelia, genetic factors that downregulated fitness status and trigger cell selection through fitness fingerprints were already identified, including ribosomal gene mutations, low dMyc levels, *scribble* defects, and reduced Dpp signaling ([Rhiner et al., 2010](#); [Merino et al., 2015](#)). Equivalent genetic modulators that initiate neuronal selection via fitness comparison are yet unknown in the neural tissue.

At the moment, it is not understood how network alterations detected in preclinical stages of AD contribute to the progression of the disease. Nevertheless, growing evidence has established a correlation between

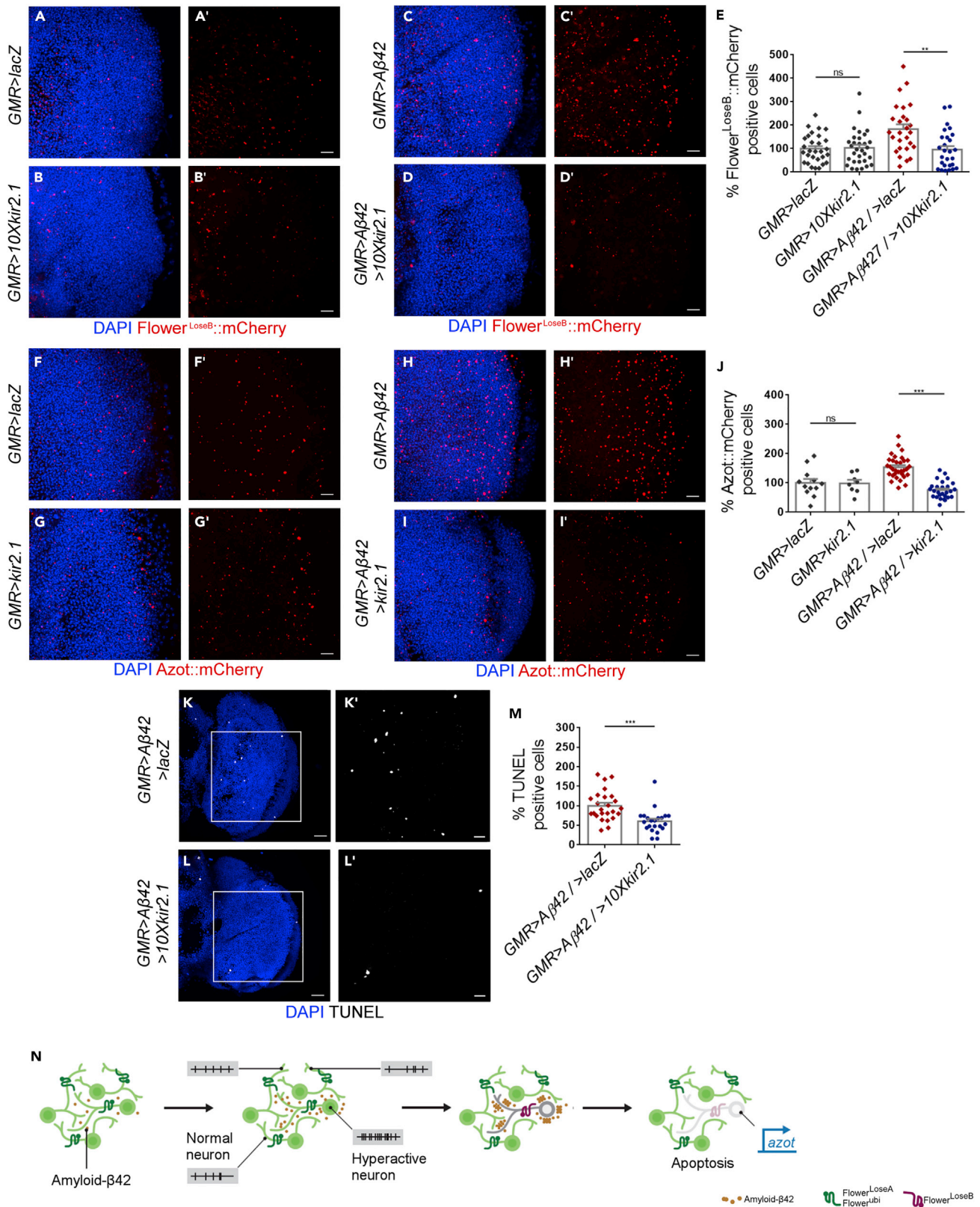


**Figure 4. Forced Silencing of Neurons Is Sufficient to Improve Cell Fitness Markers and Reduce Amyloid- $\beta$ -Induced Cell Death**

(A–D) Expression of the Flower<sup>LossE $\beta$</sup> :mCherry reporter (red) in the optic lobe of heterozygous 2-week-old flies of the following genotypes: *GMR > UAS-lacZ* (A), *GMR > 10XUAS-kir2.1* (B), *GMR > A $\beta$ 42* (C), and *GMR > A $\beta$ 42/10XUAS-kir2.1* (D). DAPI shows nuclei (blue). Scale bar, 10  $\mu$ m.

(E) Quantification of Flower<sup>LossE $\beta$</sup> :mCherry-positive cells (red) for the indicated genotypes. *GMR > UAS-lacZ* was used as reference and 100% corresponds to the mean number of Flower<sup>LossE $\beta$</sup> :mCherry-positive cells counted in this genotype. \*\*p value < 0.01, Ns: not significant, Kruskal-Wallis test with Dunn's post hoc paired multiple comparisons.

(F–I) Expression of the Azot:mCherry reporter (red) in the optic lobes of 2-week-old flies of the following genotypes: *GMR > UAS-lacZ* (F), *GMR > UAS-kir2.1* (G), *GMR > A $\beta$ 42* (H), and *GMR > A $\beta$ 42/UAS-kir2.1* (I). DAPI shows nuclei (blue). Scale bar, 10  $\mu$ m.

(J) Quantification of Azot:mCherry-positive cells (red) for the genotypes listed before in (F–I). The mean number of Azot:mCherry-positive cells counted in *GMR > UAS-lacZ* flies was assumed to be 100%. \*\*\*p value < 0.001, Ns: not significant, Kruskal-Wallis test with Dunn's post hoc paired multiple comparisons.

(K and L) TUNEL labeling of apoptotic cells (white) in the optic lobe of *GMR > A $\beta$ 42/UAS-lacZ* (K) or *GMR > A $\beta$ 42/UAS-kir2.1* flies (L). DAPI is in blue. Scale bar, 20 or 10  $\mu$ m (inset).

(M) The number of apoptotic cells labeled by TUNEL in the optic lobe of *GMR > A $\beta$ 42/UAS-lacZ* or *GMR > A $\beta$ 42/10XUAS-kir2.1* flies was quantified and plotted as shown. \*\*\*p value < 0.001, Mann-Whitney U non-parametric test.

(N) Schematic summarizing our main findings. A $\beta$ 42 generates hyperactive neurons in the *Drosophila* brain. These dysfunctional hyperactive neurons correspond to less-fit cells that are detected by the Flower-Azot pathway. Their elimination is beneficial against A $\beta$ -induced degenerative phenotypes. Data are represented as mean  $\pm$  SEM.

See also [Figure S4](#).

abnormally increased network activity and poor cognitive performance in risk groups for AD ([Bakker et al., 2012](#); [Kunz et al., 2015](#); [Miller et al., 2008](#); [Putchá et al., 2011](#)). Work done by our group and others suggests that limiting neuronal hyperactivity by pharmacological or genetic means might have staggering beneficial effects against AD progression. Treatment with the anti-epileptic drug levetiracetam was sufficient to improve cognitive performance upon reversing network and synaptic abnormalities in the hippocampus in patients at risk to develop AD and in a mouse model of AD ([Bakker et al., 2012, 2015](#); [Sanchez et al., 2012](#)). In a *Drosophila* AD model, restoring the wild-type levels of a conserved A-type K<sup>+</sup> channel (which was targeted to degradation by A $\beta$ ) decreased neuronal excitability and was sufficient to attenuate both locomotor and learning defects and to delay neurodegeneration ([Ping et al., 2015](#)). However, the same study failed to rescue A $\beta$ -induced neurodegenerative phenotypes by generally decreasing neuronal excitability with a EKO channel, a result that might be explained by EKO being a relatively weak tool to silence neurons when compared with the potent Inward-Rectifier Kir2.1 channel, for example ([Ping et al., 2015](#); [White, 2009](#)). Our findings show that counteracting A $\beta$ -induced hyperactivity by expression of the Kir2.1 channel halts neurodegeneration and enhances brain fitness markers; in alternative, promoting the removal of hyperactive neurons by fitness machinery can even rescue motor and memory decline ([Coelho et al., 2018](#)).

The report of aberrantly active neurons and circuits both in humans and animal models at early AD stages since 15 years ago has been surprising. Full-blown AD is typically characterized by neuronal silencing and death as well as synaptic dysfunction in vulnerable brain regions. The recent literature now seems to conciliate these two apparently contradictory observations by supporting a view wherein late neuronal silencing/damage might be a maladaptive consequence of early neuronal hyperactivity. A Ca<sup>2+</sup> imaging study performed in a murine model of AD revealed that the fraction of hyperactive neurons found in the hippocampus decreased with age, whereas inversely the fraction of silent neurons increased in the same brain region, suggesting a progressive compensatory inhibition of the circuit ([Busche et al., 2012](#)). In another relevant study using a *Drosophila* transgenic line, A $\beta$ 42-mediated early neuronal hyperactivity promoted pre-synaptic remodeling and later inhibition of the  $\alpha$ 7 nicotinic acetylcholine receptor signaling ([Hahm et al., 2018](#)). Our discoveries expand this general view by revealing that neuronal death might be another detrimental consequence of A $\beta$ 42-induced hyperactivity, which was overlooked by other studies so far. We found that hyperactive neurons displaying high Ca<sup>2+</sup> influx are targeted to cell death. Ca<sup>2+</sup> overload has long been associated with necrotic and apoptotic neuronal death as a consequence of toxic stimulation of NMDA receptors or leaky mutant glutamate receptors ([Dong et al., 2009](#); [Esposito et al., 2013](#); [Selimi et al., 2000](#); [Zuo et al., 1997](#)).

The fitness fingerprints mediating cell selection were recently proved to be conserved in humans, promoting competitive growth in cancer ([Madan et al., 2019](#)). In the future, it will be important to address the role of the human fitness machinery in the central nervous system during disease and aging since its manipulation might originate promising new therapeutic approaches.

**Limitations of the Study**

This study was conducted on a single organism, *Drosophila melanogaster*, that has critical limitations to model AD. *Drosophila* shows a very simple brain anatomy and homolog structures and circuits of the

human brain are not present. Moreover, complex behaviors that are impaired in AD, such as cognitive functions encoded in the hippocampus, cannot be found in the fly. The main conclusions of this study that identifies Kir2.1 as an effective repressor of A $\beta$ 42-induced neuronal death and hyperactivity need to be subjected to genetic and pharmacologic validation in mammalian systems and humans. Although the Flower protein is conserved in humans, its role as a mediator of neuronal selection in the human brain is still completely unknown. This work extensively used CaLexA expression as readout for neuronal hyperactivity. The activation of CaLexA depends on the nuclear translocation of a Ca<sup>2+</sup>-responsive transcription factor and the transcriptional activation of reporter GFP molecules; therefore, this Ca<sup>2+</sup> indicator has a slow response dynamics and poor temporal resolution. CaLexA signal is weaker and sparser than the signal of other transcriptional reporters of neuronal activity available in *Drosophila*, such as TRIC (Gao et al., 2015). As a consequence, the number of hyperactive neurons detected by CaLexA in the MB247>A $\beta$ 42 model used in this work might be underrepresented. Neuronal activity was also tested with GCaMP6. Ca<sup>2+</sup> imaging with GCaMP6 relies on rapid conformational changes and increased brightness of the modified circular GFP molecule induced by Ca<sup>2+</sup> binding (Chen et al., 2013). GCaMP6 is characterized by high sensitivity and fast kinetics, detecting subtle changes in intracellular free Ca<sup>2+</sup>, allowing the visualization of fast neuronal activity at a very short time scale (Chen et al., 2013). Owing to all these contrasting features between the two Ca<sup>2+</sup> sensors employed, the number of hyperactive neurons detected by each of them might seem divergent.

### Resource Availability

#### Lead Contact

Further information and requests for resources and reagents should be directed to and will be fulfilled by the Lead Contact, Eduardo Moreno ([eduardo.moreno@research.fchampalimaud.org](mailto:eduardo.moreno@research.fchampalimaud.org))

#### Materials Availability

This study did not generate any new reagent. The authors will provide upon request *Drosophila* strains generated previously by the laboratory or unavailable from public *Drosophila* centers. Antibodies and chemicals are available from commercial suppliers or public resources and their catalog numbers are given in the [Transparent Methods](#) section.

#### Data and Code Availability

This study did not generate new datasets or code. The original images presented here as maximum projections and image quantifications obtained are available upon request.

## METHODS

All methods can be found in the accompanying [Transparent Methods supplemental file](#).

## SUPPLEMENTAL INFORMATION

Supplemental Information can be found online at <https://doi.org/10.1016/j.isci.2020.101468>.

## ACKNOWLEDGMENTS

We thank Vasconcelos lab at Champalimaud Research for sharing equipment; Nélia Varela for assistance at the two-photon microscope; Gil Costa for help with diagrams; the Champalimaud Fly Platform for help with stock ordering and maintenance; the fly community at Champalimaud Research for sharing reagents and scientific discussions, DSHB for antibodies; the Bloomington Stock Center and the VDRC for *Drosophila* stocks. This study was funded by Fundação D. Anna de Sommer Champalimaud e Dr. Carlos Montez Champalimaud and the European Research Council (Consolidator Grant to E.M.: "Active Mechanisms of Cell Selection: From Cell Competition to Cell Fitness"). Fly platform was funded by CONGENTO LISBOA-01-0145-FEDER-022170, co-financed by FCT (Portugal) and Lisboa2020, under the PORTUGAL2020 agreement (European Regional Development Fund).

## AUTHOR CONTRIBUTIONS

D.S.C. and E.M. designed the experiments. D.S.C. conducted the experiments and analyzed data.

## DECLARATION OF INTERESTS

Authors declare no competing interests.

Received: April 9, 2020

Revised: July 15, 2020

Accepted: August 13, 2020

Published: September 25, 2020

## REFERENCES

- Aso, Y., Hattori, D., Yu, Y., Johnston, R.M., Iyer, N.A., Ngo, T.-T.B., Dionne, H., Abbott, L.F., Axel, R., Tanimoto, H., et al. (2014). The neuronal architecture of the mushroom body provides a logic for associative learning. *Elife* 3, e04577.
- Baines, R.A., Uhler, J.P., Thompson, A., Sweeney, S.T., and Bate, M. (2001). Altered electrical properties in *Drosophila* neurons developing without synaptic transmission. *J. Neurosci.* 21, 1523–1531.
- Bakker, A., Krauss, G.L., Albert, M.S., Speck, C.L., Jones, L.R., Stark, C.E., Yassa, M.A., Bassett, S.S., Shelton, A.L., and Gallagher, M. (2012). Reduction of hippocampal hyperactivity improves cognition in amnesic mild cognitive impairment. *Neuron* 74, 467–474.
- Bakker, A., Albert, M.S., Krauss, G., Speck, C.L., and Gallagher, M. (2015). Response of the medial temporal lobe network in amnesic mild cognitive impairment to therapeutic intervention assessed by fMRI and memory task performance. *Neuroimage Clin.* 7, 688–698.
- Bookheimer, S.Y., Strojwas, M.H., Cohen, M.S., Saunders, A.M., Pericak-Vance, M.A., Mazziotta, J.C., and Small, G.W. (2000). Patterns of brain activation in people at risk for Alzheimer's disease. *N. Engl. J. Med.* 343, 450–456.
- Busche, M.A., Eichhoff, G., Adelsberger, H., Abramowski, D., Wiederhold, K.-H., Haass, C., Staufenbiel, M., Konnerth, A., and Garaschuk, O. (2008). Clusters of Hyperactive Neurons Near Amyloid Plaques in a Mouse Model of Alzheimer's Disease. *Science* 321, 1686–1689.
- Busche, M.A., and Konnerth, A. (2015). Neuronal hyperactivity - a key defect in Alzheimer's disease?: neuronal hyperactivity. *BioEssays* 37, 624–632.
- Busche, M.A., Chen, X., Henning, H.A., Reichwald, J., Staufenbiel, M., Sakmann, B., and Konnerth, A. (2012). Critical role of soluble amyloid- for early hippocampal hyperactivity in a mouse model of Alzheimer's disease. *Proc. Natl. Acad. Sci. U S A* 109, 8740–8745.
- Chang, H.-F., Mannebach, S., Beck, A., Ravichandran, K., Krause, E., Frohneiler, K., Fecher-Trost, C., Schirra, C., Pattu, V., Flockerzi, V., et al. (2018). Cytotoxic granule endocytosis depends on the Flower protein. *J. Cell Biol.* 217, 667–683.
- Chen, T.-W., Wardill, T.J., Sun, Y., Pulver, S.R., Renninger, S.L., Baohar, A., Schreiter, E.R., Kerr, R.A., Orger, M.B., Jayaraman, V., et al. (2013). Ultrasensitive fluorescent proteins for imaging neuronal activity. *Nature* 499, 295–300.
- Coelho, D.S., and Moreno, E. (2019). Emerging links between cell competition and Alzheimer's disease. *J. Cell Sci* 132, jcs231258.
- Coelho, D.S., Schwartz, S., Merino, M.M., Hauert, B., Topfel, B., Tieche, C., Rhiner, C., and Moreno, E. (2018). Culling less fit neurons protects against amyloid- $\beta$ -induced brain damage and cognitive and motor decline. *Cell Rep.* 25, 3661–3673.e3.
- Dickerson, B.C., Salat, D.H., Greve, D.N., Chua, E.F., Rand-Giovannetti, E., Rentz, D.M., Bertram, L., Mullin, K., Tanzi, R.E., Blacker, D., et al. (2005). Increased hippocampal activation in mild cognitive impairment compared to normal aging and AD. *Neurology* 65, 404–411.
- Dong, X., Wang, Y., and Qin, Z. (2009). Molecular mechanisms of excitotoxicity and their relevance to pathogenesis of neurodegenerative diseases. *Acta Pharmacol. Sin.* 30, 379–387.
- Esposito, Z., Belli, L., Toniolo, S., Sancesario, G., Bianconi, C., and Martorana, A. (2013). Amyloid  $\beta$ , glutamate, excitotoxicity in Alzheimer's disease: are we on the right track? *CNS Neurosci. Ther.* 19, 549–555.
- Filippini, N., MacIntosh, B.J., Hough, M.G., Goodwin, G.M., Frisoni, G.B., Smith, S.M., Matthews, P.M., Beckmann, C.F., and Mackay, C.E. (2009). Distinct patterns of brain activity in young carriers of the APOE-epsilon4 allele. *Proc. Natl. Acad. Sci. U S A* 106, 7209–7214.
- Frere, S., and Slutsky, I. (2018). Alzheimer's disease: from firing instability to homeostasis network collapse. *Neuron* 97, 32–58.
- Gao, X.J., Riabinina, O., Li, J., Potter, C.J., Clandinin, T.R., and Luo, L. (2015). A transcriptional reporter of intracellular Ca<sup>2+</sup> in *Drosophila*. *Nat. Neurosci.* 18, 917–925.
- Grienberger, C., Rochefort, N.L., Adelsberger, H., Henning, H.A., Hill, D.N., Reichwald, J., Staufenbiel, M., and Konnerth, A. (2012). Staged decline of neuronal function in vivo in an animal model of Alzheimer's disease. *Nat. Commun.* 3, <https://doi.org/10.1038/ncomms1783>.
- Hahn, E.-T., Nagaraja, R.Y., Waro, G., and Tsunoda, S. (2018). Cholinergic homeostatic synaptic plasticity drives the progression of A $\beta$ -induced changes in neural activity. *Cell Rep.* 24, 342–354.
- Hamada, F.N., Rosenzweig, M., Kang, K., Pulver, S.R., Ghezzi, A., Jegla, T.J., and Garrity, P.A. (2008). An internal thermal sensor controlling temperature preference in *Drosophila*. *Nature* 454, 217–220.
- Igaki, T., Pastor-Pareja, J.C., Aonuma, H., Miura, M., and Xu, T. (2009). Intrinsic tumor suppression and epithelial maintenance by endocytic activation of Eiger/TNF signaling in *Drosophila*. *Dev. Cell* 16, 458–465.
- Kunz, L., Schröder, T.N., Lee, H., Montag, C., Lachmann, B., Sariyska, R., Reuter, M., Stirnberg, R., Stöcker, T., Messing-Floeter, P.C., et al. (2015). Reduced grid-cell-like representations in adults at genetic risk for Alzheimer's disease. *Science* 350, 430–433.
- Madan, E., Pelham, C.J., Nagane, M., Parker, T.M., Canas-Marques, R., Fazio, K., Shaik, K., Yuan, Y., Henriques, V., Galzerano, A., et al. (2019). Flower isoforms promote competitive growth in cancer. *Nature* 572, 260–264.
- Masuyama, K., Zhang, Y., Rao, Y., and Wang, J.W. (2012). Mapping neural circuits with activity-dependent nuclear import of a transcription factor. *J. Neurogenet.* 26, 89–102.
- McGuire, S.E., Mao, Z., and Davis, R.L. (2004). Spatiotemporal gene expression targeting with the TARGET and gene-switch systems in *Drosophila*. *Sci. STKE* 2004, pl6.
- Menéndez, J., Pérez-Garijo, A., Calleja, M., and Morata, G. (2010). A tumor-suppressing mechanism in *Drosophila* involving cell competition and the Hippo pathway. *Proc. Natl. Acad. Sci. U S A* 107, 14651–14656.
- Merino, M.M., Rhiner, C., Portela, M., and Moreno, E. (2013). "Fitness fingerprints" mediate physiological culling of unwanted neurons in *Drosophila*. *Curr. Biol.* 23, 1300–1309.
- Merino, M.M., Rhiner, C., Lopez-Gay, J.M., Buechel, D., Hauert, B., and Moreno, E. (2015). Elimination of unfit cells maintains tissue health and prolongs lifespan. *Cell* 160, 461–476.
- Merino, M.M., Levayer, R., and Moreno, E. (2016). Survival of the fittest: essential roles of cell competition in development, aging, and cancer. *Trends Cell Biol.* 26, 776–788.
- Miller, S.L., Celone, K., DePeau, K., Diamond, E., Dickerson, B.C., Rentz, D., Pihlajamäki, M., and Sperling, R.A. (2008). Age-related memory impairment associated with loss of parietal deactivation but preserved hippocampal activation. *Proc. Natl. Acad. Sci. U S A* 105, 2181–2186.
- Mondadori, C.R.A., Buchmann, A., Mustovic, H., Schmidt, C.F., Boesiger, P., Nitsch, R.M., Hock, C., Streffer, J., and Henke, K. (2006). Enhanced brain activity may precede the diagnosis of Alzheimer's disease by 30 years. *Brain* 129, 2908–2922.
- Moreno, E., Basler, K., and Morata, G. (2002). Cells compete for decapentaplegic survival factor

to prevent apoptosis in *Drosophila* wing development. *Nature* 416, 755–759.

Moreno, E., and Basler, K. (2004). dMyc transforms cells into super-competitors. *Cell* 117, 117–129.

Moreno, E., Fernandez-Marrero, Y., Meyer, P., and Rhiner, C. (2015). Brain regeneration in *Drosophila* involves comparison of neuronal fitness. *Curr. Biol.* 25, 955–963.

Palop, J.J. (2009). Epilepsy and cognitive impairments in Alzheimer disease. *Arch. Neurol.* 66, 435.

Palop, J.J., and Mucke, L. (2010). Amyloid-beta-induced neuronal dysfunction in Alzheimer's disease: from synapses toward neural networks. *Nat. Neurosci.* 13, 812–818.

Petrova, E., López-Gay, J.M., Rhiner, C., and Moreno, E. (2012). Flower-deficient mice have reduced susceptibility to skin papilloma formation. *Dis. Model Mech.* 5, 553–561.

Ping, Y., Hahm, E.-T., Waro, G., Song, Q., Vo-Ba, D.-A., Licursi, A., Bao, H., Ganoe, L., Finch, K., and Tsunoda, S. (2015). Linking  $\alpha\beta 42$ -induced hyperexcitability to neurodegeneration, learning and motor deficits, and a shorter lifespan in an Alzheimer's model. *PLoS Genet.* 11, e1005025.

Putcha, D., Brickhouse, M., O'Keefe, K., Sullivan, C., Rentz, D., Marshall, G., Dickerson, B., and Sperling, R. (2011). Hippocampal hyperactivation associated with cortical thinning in Alzheimer's disease signature regions in non-demented elderly adults. *J. Neurosci.* 31, 17680–17688.

Quiroz, Y.T., Budson, A.E., Celone, K., Ruiz, A., Newmark, R., Castrillón, G., Lopera, F., and Stern, C.E. (2010). Hippocampal hyperactivation in presymptomatic familial Alzheimer's disease. *Ann. Neurol.* 68, 865–875.

Reiman, E.M., Quiroz, Y.T., Fleisher, A.S., Chen, K., Velez-Pardo, C., Jimenez-Del-Rio, M., Fagan, A.M., Shah, A.R., Alvarez, S., Arbelaez, A., et al. (2012). Brain imaging and fluid biomarker analysis

in young adults at genetic risk for autosomal dominant Alzheimer's disease in the presenilin 1 E280A kindred: a case-control study. *Lancet Neurol.* 11, 1048–1056.

Rodrigues, A.B., Zoranovic, T., Ayala-Camargo, A., Grewal, S., Reyes-Robles, T., Krasny, M., Wu, D.C., Johnston, L.A., and Bach, E.A. (2012). Activated STAT regulates growth and induces competitive interactions independently of Myc, Yorkie, Wingless and ribosome biogenesis. *Development* 139, 4051–4061.

Rhiner, C., López-Gay, J.M., Soldini, D., Casas-Tinto, S., Martin, F.A., Lombardía, L., and Moreno, E. (2010). Flower forms an extracellular code that reveals the fitness of a cell to its neighbors in *Drosophila*. *Dev. Cell* 18, 985–998.

Rudinskiy, N., Hawkes, J.M., Betensky, R.A., Eguchi, M., Yamaguchi, S., Spires-Jones, T.L., and Hyman, B.T. (2012). Orchestrated experience-driven Arc responses are disrupted in a mouse model of Alzheimer's disease. *Nat. Neurosci.* 15, 1422–1429.

Sanchez, P.E., Zhu, L., Verret, L., Vossel, K.A., Orr, A.G., Cirrito, J.R., Devidze, N., Ho, K., Yu, G.-Q., Palop, J.J., et al. (2012). Levetiracetam suppresses neuronal network dysfunction and reverses synaptic and cognitive deficits in an Alzheimer's disease model. *Proc. Natl. Acad. Sci. U S A* 109, E2895–E2903.

Selimi, F., Doughty, M., Delhaye-Bouchaud, N., and Mariani, J. (2000). Target-Related and intrinsic neuronal death in *lurcher* mutant mice are both mediated by caspase-3 activation. *J. Neurosci.* 20, 992–1000.

Sperling, R.A., LaViolette, P.S., O'Keefe, K., O'Brien, J., Rentz, D.M., Pihlajamaki, M., Marshall, G., Hyman, B.T., Selkoe, D.J., Hedden, T., et al. (2009). Amyloid deposition is associated with impaired default network function in older persons without dementia. *Neuron* 63, 178–188.

Stargardt, A., Swaab, D.F., and Bossers, K. (2015). Storm before the quiet: neuronal hyperactivity

and A $\beta$  in the presymptomatic stages of Alzheimer's disease. *Neurobiol. Aging* 36, 1–11.

Vincent, J.-P., Kolahgar, G., Gagliardi, M., and Piddini, E. (2011). Steep differences in wingless signaling trigger Myc-independent competitive cell interactions. *Dev. Cell* 21, 366–374.

Vossel, K.A., Beagle, A.J., Rabinovici, G.D., Shu, H., Lee, S.E., Naasan, G., Hegde, M., Cornes, S.B., Henry, M.L., Nelson, A.B., et al. (2013). Seizures and epileptiform activity in the early stages of Alzheimer disease. *JAMA Neurol.* 70, 1158–1166.

Vossel, K.A., Ranasinghe, K.G., Beagle, A.J., Mizuiri, D., Honma, S.M., Dowling, A.F., Darwish, S.M., Van Berlo, V., Barnes, D.E., Mantle, M., et al. (2016). Incidence and impact of subclinical epileptiform activity in Alzheimer's disease. *Ann. Neurol.* 80, 858–870.

White, B. (2009). Neurotrapping: cellular screens to identify the neural substrates of behavior in *Drosophila*. *Front. Mol. Neurosci.* 2, 20.

Xue, L., Zhang, Z., McNeil, B.D., Luo, F., Wu, X.-S., Sheng, J., Shin, W., and Wu, L.-G. (2012). Voltage-dependent calcium channels at the plasma membrane, but not vesicular channels, couple exocytosis to endocytosis. *Cell Rep.* 1, 632–638.

Yao, C.-K., Lin, Y.Q., Ly, C.V., Ohya, T., Haueter, C.M., Moiseenkova-Bell, V.Y., Wensel, T.G., and Bellen, H.J. (2009). A synaptic vesicle-associated Ca<sup>2+</sup> channel promotes endocytosis and couples exocytosis to endocytosis. *Cell* 138, 947–960.

Zott, B., Busche, M.A., Sperling, R.A., and Konnerth, A. (2018). What happens with the circuit in Alzheimer's disease in mice and humans? *Annu. Rev. Neurosci.* 41, 277–297.

Zuo, J., De Jager, P.L., Takahashi, K.A., Jiang, W., Linden, D.J., and Heintz, N. (1997). Neurodegeneration in *Lurcher* mice caused by mutation in  $\delta 2$  glutamate receptor gene. *Nature* 388, 769–773.

iScience, Volume 23

## Supplemental Information

**Neuronal Selection Based on Relative Fitness**

**Comparison Detects and Eliminates**

**Amyloid- $\beta$ -Induced Hyperactive Neurons in *Drosophila***

**Dina S. Coelho and Eduardo Moreno**

SUPPLEMENTAL INFORMATION Contents

Within this file:

Supplemental Figures S1-S4 and Legends to Supplemental Figures

Transparent Methods

Supplemental References

In separate files:

Supplemental Video S1 (separate .avi file)

Supplemental Video S2 (separate .avi file)

## Supplemental Figures

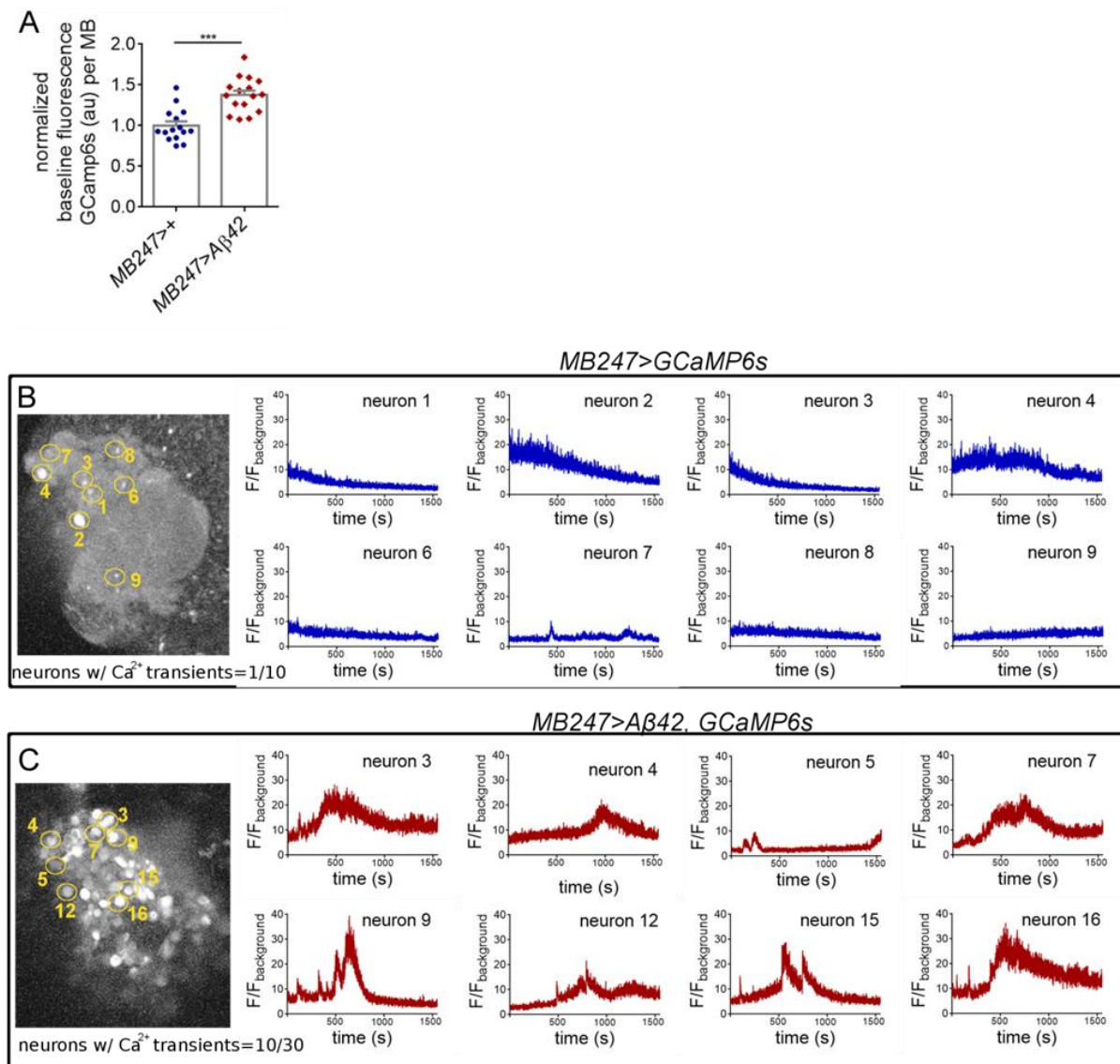


**Figure S1. Two-photon Ca<sup>2+</sup> imaging of *ex-vivo* MB247>A $\beta$ 42 brains using GCaMP6s. Related to Figure 1.**

(A) Mean intensity value of *GCaMP6s* fluorescence measured per mushroom body calyx in non-stimulated *ex-vivo* brains at baseline. Intensity values for MB247>A $\beta$ 42 brains were normalized to the intensity values of control MB247>+ brains. \*\*\*P<0.001, unpaired Student's t-test with Welch's correction.

(B) Plots depicting oscillations of *GCaMP6s* fluorescence recorded overtime by two-photon imaging for representative individual neurons in a plan of the mushroom body in MB247>+ *ex-vivo* brains. *GCaMP6s* fluorescence was acquired every 0.5s and normalized to the background fluorescence at each time point.

(C) Plots depicting oscillations of *GCaMP6s* fluorescence recorded overtime by two-photon imaging for representative individual neurons in a plan of the mushroom body in MB247>A $\beta$ 42 *ex-vivo* brains. *GCaMP6s* fluorescence was acquired every 0.5s and normalized to the background fluorescence at each time point.

Experiments represented in B and C were replicated more than 2 independent times and similar results were obtained.

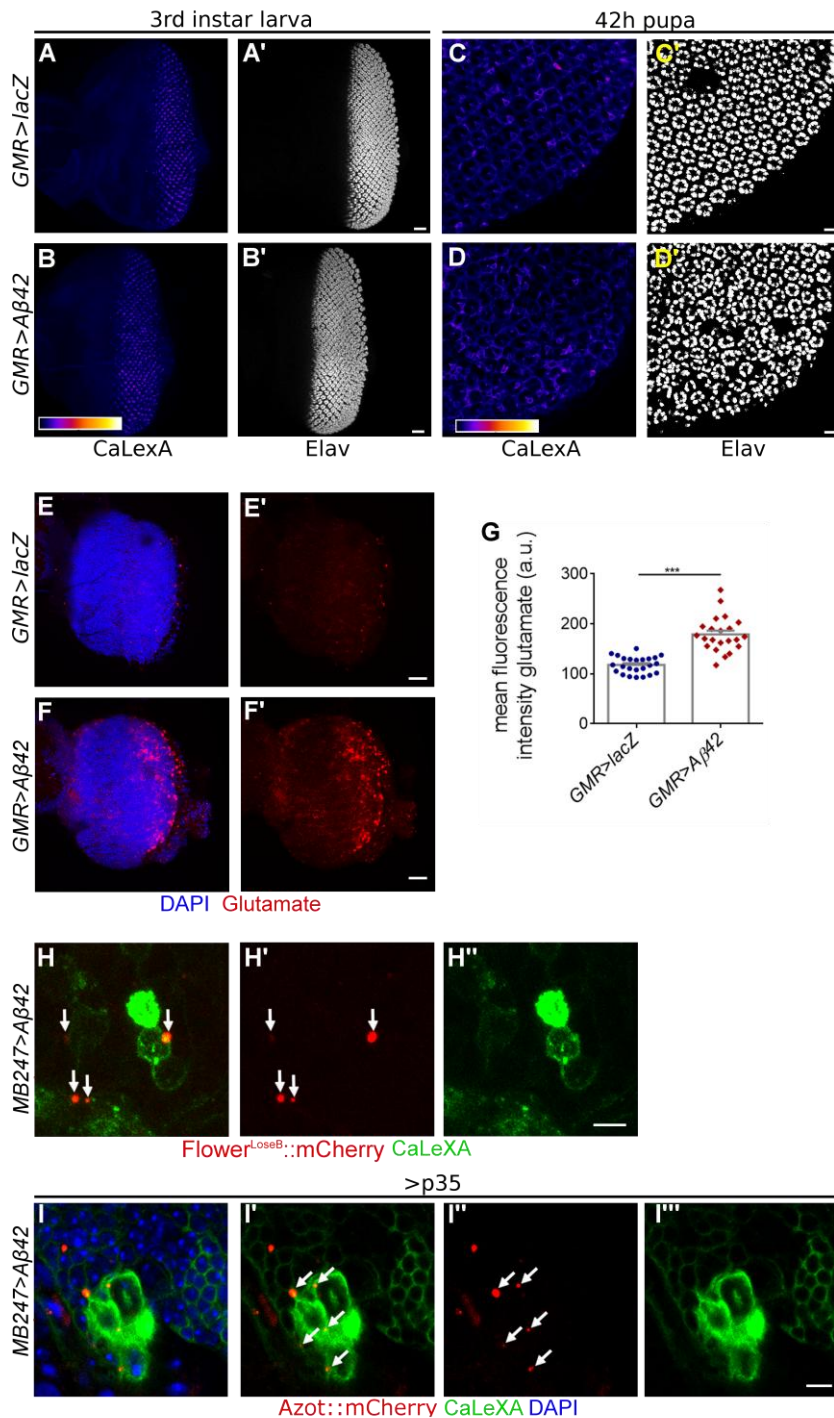


**Figure S2. CaLexA pattern in neuronal tissue of the larva, pupa or adult in the presence of heterologous Aβ42. Related to Figure 1.**

(A, B) Expression of the CaLexA system (pseudocolored fire) in the eye imaginal disc of *GMR>+* (A) or *GMR>Aβ42* (B) third instar larvae. Neuronal nuclei marked by the anti-Elav antibody are in white. Scale bar, 20μm.

(C,D) Expression of the CaLexA system (pseudocolored fire) in the pupal retina of *GMR>+* (C) or *GMR>Aβ42* individuals (D), at 42h pupation. Nuclei marked by Elav antibody are in white. Scale bar, 10μm.

(E,F) Immunohistochemistry with anti-glutamate antibody (red) in the optic lobe of *GMR>Aβ42* (F) or *GMR>lacZ* (E) flies at 15 days of age. Nuclei are in blue. Scale bar: 20μm.

(G) Graph represents the mean fluorescence intensity for anti-glutamate staining per optic lobe for the genotypes *GMR>Aβ42* or *GMR>lacZ*. \*\*\*P<0.001, unpaired Student's t-test with Welch's correction.

(H) Kenyon cells activating CaLexA (green) exhibit positive signal for the *Flower<sup>LoseB</sup>::mCherry* (red) fusion protein at membranes of the soma and neuropile projections (arrows).

(I) Presence of *Azot::mCherry* positive-foci (red) at the membrane of Kenyon cells which are inducing the expression of the CaLexA system (green) - arrows. Apoptosis of less fit neurons is prevented in these flies by driving a *UAS-p35* construct.



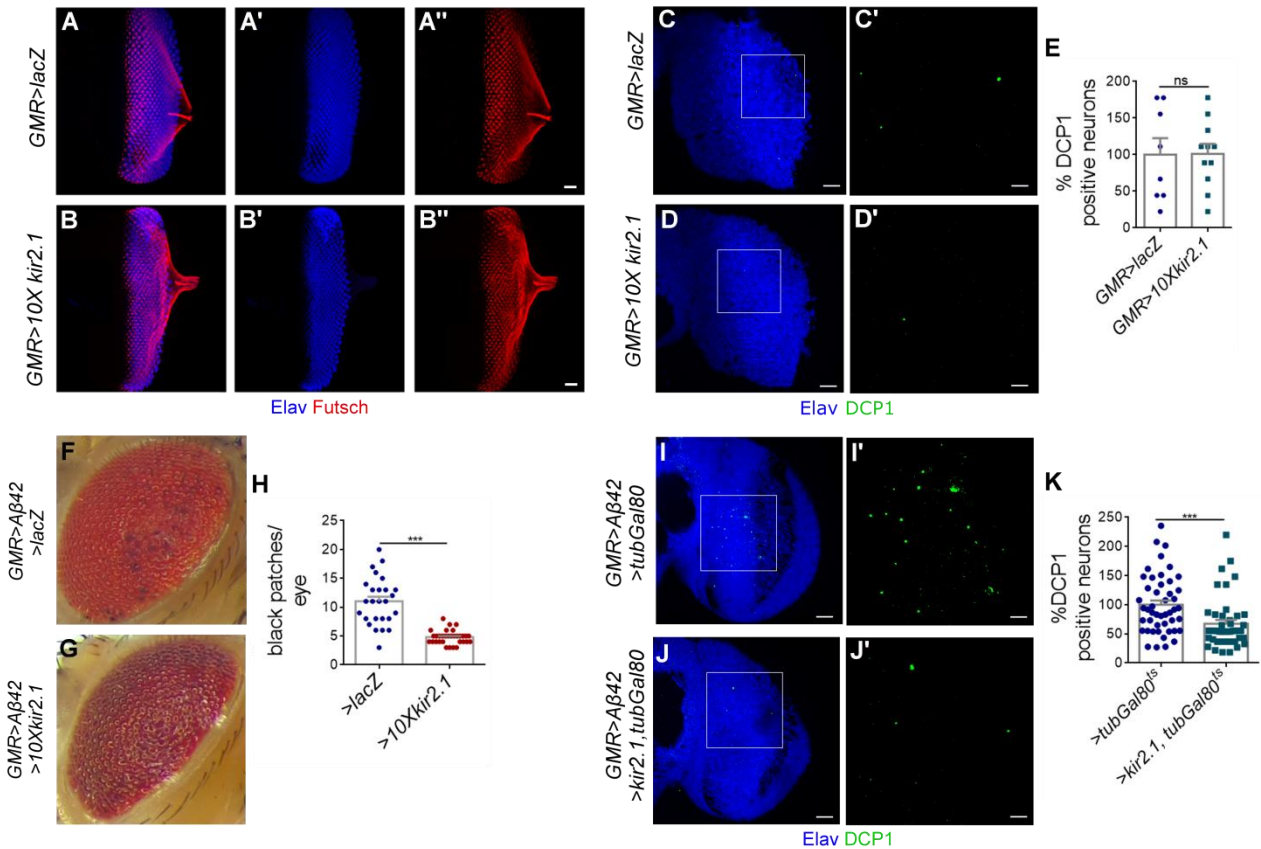


**Figure S4. Ectopic expression of Kir2.1 reduces amyloid- $\beta$ -induced cell death. Related to Figure 4.**

(A-B) Staining for the neuronal markers Elav (blue) and Futsch (red) in eye imaginal discs of *GMR>UASlacZ* (A) or *GMR>10XUAS-kir2.1* (B) third instar larva. Scale bar: 20 $\mu$ m

(C,D) Expression of *10XUAS-kir2.1* under the control of the *GMR-Gal4* driver does not perturb differentiation of neurons and does not cause increased apoptosis in the optic lobe. DCP1 marks dying cells (green) and Elav labels differentiated neurons (blue). Scale bar: 20 $\mu$ m or 8  $\mu$ m in the inset.

(E) Quantification of apoptotic cells marked by DCP1 (green) in the optic lobe of *GMR>UASlacZ* (C) or *GMR>10XUAS-kir2.1* (D) flies. Ns: no significant, Mann-Whitney U non-parametric test.

(F,G) Degenerative eye phenotype of 4-5 days old adult flies raised at 25°C for the following genotypes: *GMR>Aβ42 / UAS-lacZ* (F) and *GMR>Aβ42 / 10XUAS-kir2.1* (G).

(H) Quantification of the number of black necrotic patches counted per eye for the genotypes indicated before in (F,G). \*\*\*P value < 0.001, Krustal-Wallis test with Dunn's post-hoc test.

(I-K) Representative images of apoptotic cells marked by DCP1 (green) in the optic lobe of *GMR>Aβ42 / >UAS-tubGal80ts* (I) or *GMR>Aβ42 / UASkir2.1, tubGal80ts* (J) flies and respective quantification (K). To restrict Gal4 expression to adulthood, flies were raised at 18°C and transferred to 30°C 1-2 days after eclosion. Neurons are shown in blue. Scale bar: 20 $\mu$ m or 6 $\mu$ m in the inset. \*\*\*P value < 0.001, Mann-Whitney U non-parametric test.

Error bars show standard error mean.

## Transparent Methods

### Genetics

All experimentation was conducted on *Drosophila melanogaster*. The number of flies used was the minimum necessary to achieve the objectives and the best practices were employed. Flies were treated in a humane manner, using CO<sub>2</sub> as anesthetic and were kept according to applicable European and Institutional guidelines.

All stocks were maintained on a standard cornmeal/molasses medium at 25°C in a 12 hr light/dark cycle, unless otherwise indicated. Male flies were used as subjects in all experiments. The following stocks were obtained from the Bloomington stock center: *GMR-Gal4* (second chr, RRID: BDSC\_1104); *20XUAS-GCaMP6s* (second chr., BDSC #42746), *UAS-diap1* (second chr., RRID: BDSC\_63820); *UAS-lacZ* (second chr., RRID: BDSC\_3955); *MB247-Gal4* (third, RRID: BDSC\_50742), *UAS-p35* (second chr., RRID: BDSC\_5072). The *GMRGal4>(2x)UAS-Aβ42* model was generated for Casas-Tinto et al., 2011. The following transgenic lines were described in previous publication of our laboratory: *flower<sup>LoseB</sup>::mCherry KI* (third Chr.) and *azot::mCherry* reporter line (third chr.) in Coelho et al., 2018; *UAS-flower<sup>LoseA/B</sup> long hairpin RNAi* in Merino et al., 2013; *UAS-flower<sup>LoseA</sup>* in Rhiner et al., 2010. The CaLexA system whose complete genotype is *w;lexAop-CD8-GFP-2A-CD8-GFP/CyO; UAS-mLexA-VP16-NFATC(H-2), LexAop-CD2-GFP/TM6b* was designed for Masuyama et al., 2012. Flies carrying the translational reporter *Flower<sup>LoseB</sup>::Myc* or the point mutation *UAS-flower<sup>LoseA[E79Q]</sup>* were gifts from Hugo Bellen (Yao et al., 2009). The *UAS-fve dsRNA* transgenic line was obtained from the Vienna Drosophila Resource Center (second chr, GD collection VDRC #39596, RRID: FlyBase\_FBst0463114). The stock *10XUAS-kir2.1::EGFP* was generated by the Gwyneth M.Card lab (von Reyn et al., 2014). Additional stocks were obtained from other research laboratories at Champalimaud: *UAS-trpAI* (second chr.) was obtained from the Chiappe lab; *UAS-kir2.1* inserted on the second chromosome and the recombinant lines *tubGal80,UAS-kir2.1* and *chat-Gal4,UAS-GFP* were obtained from the Vasconcelos lab.

### Neuronal activation and neuronal silencing

To activate TRPA1, flies were collected 1 day after eclosion and transferred to 30°C for 4days until dissection. Control non-activated flies were kept at 22°C for the same time period.

When using the *tubGAL80<sup>ΔS</sup>* transgene, flies were raised at 18°C and placed at 30°C shortly after eclosion for Gal4 expression and *kir2.1* induction.

When monitoring neuronal activity with GCaMP6s or CaLexA, vials from different experimental groups were always kept side-by-side to ensure all flies were subjected to same environmental stimuli prior to experiments.

### Immunohistochemistry and image acquisition

For clone induction, larvae were given a heat shock at 37°C, 48h or 72h before dissection. For pupal dissections, white prepupae (0hr) were collected and maintained at 25°C for 42h. For adult brain dissections, males were collected 0-1 days after eclosion and maintained at 25°C until the required age. Dissections were performed in chilled PBS, samples were fixed for 30min in formaldehyde (4% v/v in PBS) at room temperature and washed for 60min with PBT 0,4% Triton. For blocking, samples were incubated for 1h at room temperature in 10% normal goat serum (Sigma Aldrich, Cat# G9023) in PBT and incubated overnight with the primary antibody diluted in the same solution at 4°C. The following antibodies were used: rat anti-Elav (1:50; Developmental Studies Hybridoma Bank, DSHB, Cat#7E8A10, RIDD AB\_528218); mouse anti-Futsch (1:200, DSHB Cat#22C10, RRID:AB\_528403); polyclonal anti-Myc-tag (1:50; Cell Signaling Cat#2272; RRID:AB\_10692100), cleaved DCP1 (1:100, Cell Signaling Cat#9578,

RRID:AB\_2721060), chicken anti-GFP (1:500 Abcam Cat#ab13970, RRID:AB\_30079813970). TUNEL staining (Roche Cat#3333574001 and Roche Cat#11093070910) was performed according to the supplier's protocol and modified as previously (Lolo et al., 2012). Samples were mounted in Vectashield (Vectorlab Cat#H-1200) and imaged on a Zeiss LSM 880 using a 20X dry objective or a 40X oil objective.

### Calcium imaging experiments with GCaMP6

For two-photon  $\text{Ca}^{2+}$  imaging experiments, flies expressed the  $\text{Ca}^{2+}$  indicator GCaMP6s in the mushroom body. To obtain *ex-vivo* preparations of the adult brain, flies were dissected in a saline solution composed of 108mM NaCl, 5mM KCl, 4mM  $\text{NaHCO}_3$ , 1mM  $\text{NaH}_2\text{PO}_4$ , 5mM Trehalose\* $2\text{H}_2\text{O}$ , 10mM sucrose and 5mM HEPES. Isolated brains were immediately transferred to a coated Petri dish and covered with the same saline solution supplemented with 2mM  $\text{CaCl}_2*2\text{H}_2\text{O}$  and 8.2mM  $\text{MgCl}_2*6\text{H}_2\text{O}$ .

An Ultima two-photon laser-scanning microscope from Bruker (Billerica) and a Coherent Chameleon XR laser were used for imaging. Images were acquired with an Olympus BX61 microscope equipped with a 40X 0.8 NA objective. The image was zoomed to allow the selection of a region of interest (ROI) including the mushroom body calyx. No stimulation was performed. A z-stack of the mushroom body calyx was acquired for each sample at time=0s and without stimulation to obtain a measure of GCaMP6s fluorescence at baseline for each genotype. In addition, we recorded videos of the spontaneous oscillations of GCaMP6s fluorescence by acquiring images of the same ROI every 0.5s in a single plan for 30min.

### Image analysis and Statistics

Image quantification and fluorescent intensity measurements were done with Fiji.

To determine GCaMP6s fluorescence, we delineated by hand and around the observable soma of each neuron a second ROI. We measured the baseline fluorescence per neuronal soma at time =0s and then calculated the mean intensity value at each time frame. To calculate the normalized oscillation in the relative fluorescence of *GCaMP6s* overtime, we divided the intensity fluorescence per each neuronal soma in the  $n^{\text{th}}$  frame by the background intensity of the same frame.

We quantified CaLexA signal on 30 $\mu\text{m}$ -wide maximum projections that included almost the total width of the mushroom body calyx in males at 10days (except for data in Fig.2A where males with 5, 10 or 15days were used). When acquiring images, we adjusted the gain so that the genotype with the strongest signal did not saturate the dynamic range of the PMT detector, and we imaged all the brains with the same settings and as close as possible time-wise. To quantify the number of saturated pixels for CaLexA as depicted in Fig.1, a histogram displaying the distribution of number of pixels per fluorescence intensity value was obtained for each z-projection. Pixels with intensities values above 75% of the maximum value were counted as saturated. We scored as CaLexA-activating neurons as shown in Fig2, Kenyon cells exhibiting intense signal of GFP in the soma comparing to other neurons in the vicinity. The number of CaLexA-activating neurons was scored blindly across different genotypes. The number of hyperactive neurons scored for each sample was divided by the mean number of CaLexA-positive neurons present in the control genotype of the same experimental replicate and represented as a percentage of it. In the end, results from all experimental replicates were pooled for each genotype and mean and SEM were calculated.

The number of positive cells for FlowerLoseB::mCherry or Azot::mCherry signal represented in Figures 3 or 4 was determined with the FIJI tool 'Find Maxima' in maximum-intensity projections of the optic lobe. Z-stacks spanned approximately 40 $\mu\text{m}$  of each optic lobe starting from the anterior side of the brain. Noise signal was removed

beforehand with a Gaussian blur filter ( $\sigma = 1$  or  $\sigma = 1.5$ ). Comparisons were made between data collected either from parallel experiments, with exactly the same solutions, timeline, and imaging conditions, or from different batches of experiments normalized to a common control. For example, data for Fig. 3 were collected separately, but within each batch there was always one group of UAS-lacZ at 30°C, whose signal served as the common denominator.

The mean intensity fluorescence for glutamate in the optic lobe (or for GCaMP6s in the mushroom body) was determined by measuring the mean intensity per pixel in ROIs with the same size.

In images illustrating co-localization experiments, we show single slices (**Fig. 1K, Fig. 1L, Fig. 2B, Fig.S2H, Fig.S2I, Fig.S3D, Fig.S3E**) while for the rest of the panels, we show maximum-projections (with the same thickness when comparing between different genotypes).

All statistical analyses were performed using GraphPad Prism software version 6.0 (GraphPad Software). The number of Flower<sup>LoseB</sup>::mCherry and Azot::mCherry positive cells in the adult optic lobes (**Fig. 3F,J; Fig. 4E,J**) and the number of black patches in the adult eye (**Fig.S4H**) were analyzed with a Kruskal-Wallis test with Dunn's post-hoc paired comparisons. Mann-Whitney U non-parametric tests were performed to determine significant differences between two groups for the following variables: baseline fluorescence of GCaMP6s per neuron (**Fig.1C**), number of saturated CaLexA pixels (**Fig.1G**), number of TUNEL-positive cells in the adult optic lobe (**Fig. 4M**), clone number per wing pouch (**Fig. S3C**) and percentage of DCP-1 positive cells (**Fig.2F, Fig. S4C and Fig.S4K**). We compared the number of CaLexA-labelled neurons across time points with one-way ANOVA and Holm-Sidak's multiple comparisons tests (**Fig.2A**). An unpaired Student's t-test with Welch's correction was used to analyze the number of CaLexA-activating neurons (**Fig.2E, J**), the normalized baseline fluorescence of GCaMP6s per mushroom body (**Fig. S1A**), the fluorescence intensity of glutamate (**Fig. S2G**) number of TUNEL-positive cells in the adult optic lobe (**Fig.3M,P**).

All the p-values are two tailed and all graphs are displayed as mean  $\pm$  standard error.

### Supplemental References

Casas-Tinto, S., Zhang, Y., Sanchez-Garcia, J., Gomez-Velazquez, M., Rincon-Limas, D.E., and Fernandez-Funez, P. (2011). The ER stress factor XBP1s prevents amyloid- neurotoxicity. *Human Molecular Genetics* 20, 2144–2160.

von Reyn, C.R., Breads, P., Peek, M.Y., Zheng, G.Z., Williamson, W.R., Yee, A.L., Leonardo, A., and Card, G.M. (2014). A spike-timing mechanism for action selection. *Nat Neurosci* 17, 962–970.